Two-phase nozzles performances CFD modeling for low-grade heat to power generation: mass transfer models assessment and a novel transitional formulation

Egoi Ortego Sampedro, Florent Breque, Maroun Nemer

Two-phase nozzles performances CFD modeling for low-grade heat to power generation: mass transfer models assessment and a novel transitional formulation

Keywords

Low grade heat valorization; motive nozzle efficiency; two-phase flow; interfacial area density; thermal phase change model; ejector ; ORC

Highlights

- Four phase change models were compared in a two fluids metastable flow description
- A novel transitional area density formulation was explored for motive flash nozzles
- Simultaneous calibration of flow rate and velocity was not possible for some models
- The best models are the ones based on multiple and non-redundant calibration terms

Abstract

The use of two-phase nozzles for low-grade heat valorization by electricity production increases the energy recovery rate using Trilateral Flash or Wet to Dry cycles. A model benchmark for nozzle flow rate and efficiency estimation was conducted on experimental data from the literature. These data come from a series of tests made on geothermal energy production water two-phase nozzles. A new transitional bubble-to-droplet interfacial area density formulation (TA-BD model) is presented by the paper. It is compared to three models from literature. Two nozzles operating with different inlet and outlet conditions were modeled. The calibration flexibility and the robustness of the models are discussed in association with physical analysis. The paper shows how the models using single or redundant adaptation parameters fail to provide good results simultaneously on flow rate and efficiency. It appeared that the TA-BD model is the more flexible and robust. The Homogeneous Relaxation Model (HRM) model gives also good results. Furthermore, TA-BD model gives the lowest average discrepancies. Especially at the best efficiency point of the first test case, TA-BD model shows less than 1% discrepancy where the HRM model has 18% discrepancy in efficiency. The TA-BD model appeared to be easier to calibrate than the HRM model. Finally, regarding the proposed TA-BD model, the sensitivity to the geometry and operating conditions shows that the interfacial area density formulation could be completed to include the effect of nozzle's section profile, the effect of the inlet temperature on bubbles number density, and the effect of outlet pressure on the droplets number density.

Nomenclature

Roman characters

A	interfacial area density [m^{-1}]
a	empirical coefficient for HRM model
b	empirical coefficient for HRM model
C_D	drag coeffiicient
C_P	isobaric heat capacity [J kg^{-1} K^{-1}]
D_I	drag force[N m^{-3}]
D_T	thermal diffusivity [m^2 s^{-1}]
h^t	total enthalpy [J kg^{-1}]
h_i	interfacial heat transfer coefficient [W $m^{-2}K^{-1}$]
Ja	Jakob number
K	relaxation coefficient
l_c	interfacial length scale [m]
N	number density [m^{-3}]
M	interface forces [N m^{-3}]
P	pressure [Pa]
P_e	Peclet number
P_r	Prandtl number
$\dot{q}_1$	interfacial heat transfer [W m^{-3}]
R_g	universal gas constant [kg $kmol^{-1}$]
s	entropy [J kg^{-1} K^{-1}]
T	temperature [K]
U	velocity [m s^{-1}]
vof	volume fraction
x	quality

Greek characters

α	volume fraction
Γ	volumetric mass flow rate [$kg\ m^{-3}s^{-1}$]
η	isentropic efficiency
θ	relaxation time [s]
λ	thermal conductivity [W m^{-1}]
λ_{acc}	accomodation coefficient
μ	dynamic viscosity [Pa s]
ρ	density [kg m^{-3}]
τ	viscous stresses
ϕ	mass transfer potential
ψ	pressure ratio

Subscripts

1	Liquid phase
2	gas phase
b	bubble
$crit$	critical
d	droplet
gl	gas to liquid
i	interfacial
in	inlet
mix	mixture
ml	methastable liquid
out	outlet
s	isentropic
sat	saturated
sg	saturated gas
sl	saturated liquid
slu	slug
T	Taylor

p	first phase
p'	second phase
ΔP	Pressure based model

Acronyms

CFD	Computational Fluid Dynamics
HK	Hertz- Knudsen
HRM	Homogeneous Relaxation Model
SC	Sub Cooling
Sch	Super Heat
TA-BD	Thermal Bubble to Droplet
TFC	Trilateral Flash Cycle
VOF	Volume fraction
WDC	Wet to Dry Cycle

1. Introduction

Electricity production from waste-heat is a promising solution for the reduction of fossil fuels usage. Advanced Trilateral Flash Cycles (TFC) and Wet to Dry Cycles (WDC) can increase the profitability of low-grade heat based production plants [1]. Compared to a Rankin cycle, TFC and WDC cycles present a higher output power density thanks to the better matching between the hot source and the working fluid temperatures at the boiler [3]. An example of a trilateral flash cycle in a temperature-entropy diagram is shown in Figure 1. Since the flow rate of the sensible hot stream of classical waste-heat sources is finite, the ideal cycle leading to the maximum output power has a triangular shape.

In such cycles the key element is the two-phase turbine; it can produce power from an initially sub-cooled or saturated flashing liquid stream [3]. An example of a two-phase nozzle and turbine arrangement is presented in Figure 2.

The renewed interest in these types of cycles and turbines is attested by recent publications on advanced Organic Rankin Cycles (ORC) like the experimental work of Iqbal et al. on two-phase impulse turbines [1] or the numerical exploration of White on wet-to-dry cycles [4].

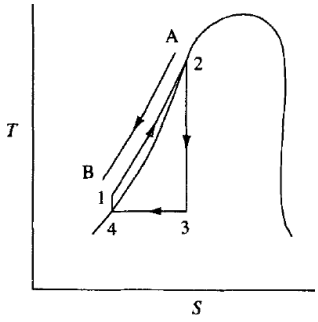

Figure 1 : trilateral flash cycle [2]

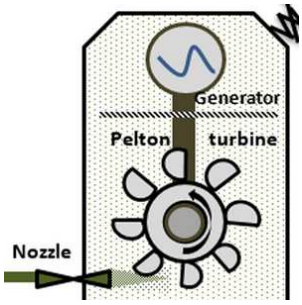

Figure 2 : two-phase nozzle and impulsion turbine arrangement [1]

In such systems, the main part of the expansion occurs in the two-phase nozzle. The nozzle can be static [1] or rotating like in the numerical exploration of the very low-temperature turbine of Rane & He [5]. Its behavior modeling is fundamental for such systems design and optimization.

The general behavior of the flashing flow in a motive nozzle is presented in Figure 3. The flow's pressure and velocity evolutions in the nozzle are represented by the side ''A'' of the figure; the nozzle inlet is in general in a slightly sub-cooled state then, when flowing through the convergent, liquid accelerates so the static pressure decreases and finally, cavitation occurs at the throat. In the divergent, the flow accelerates continuously up to the outlet (in adapted flow conditions). The side B of the figure shows, in a P-h diagram, the actual expansion; it follows a path somewhere between isenthalpic and isentropic expansions.

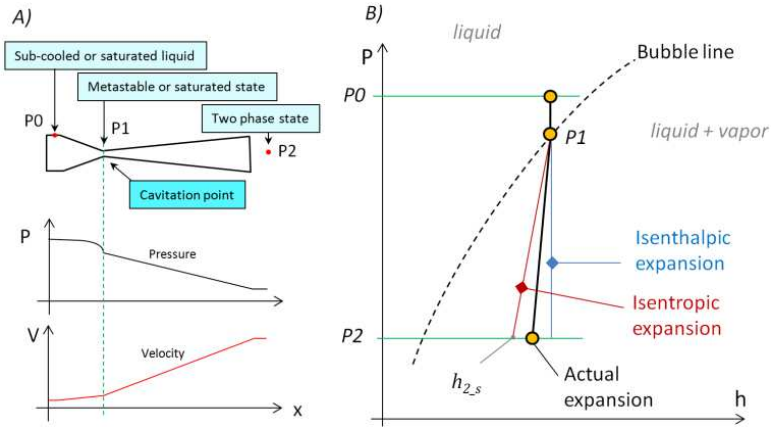

Figure 3 : general motive nozzle behavior

The nozzle efficiency is related to the isentropic velocity (assuming negligible inlet velocity) as follows:

$$\eta = \frac{V_{\vec{gl}}^2}{V_m^2} = \frac{V_{\vec{gl}}^2}{2\left(h_{2\_s}(P_2, s_0) - h_0(P_0, T_0)\right)}$$

The actual outlet velocity corresponds to the liquid and vapor mixture velocity ($V_{\vec{gl}}$). It depends on several factors such as the nozzle shape, the operating conditions, the metastability degree, the outlet vapor void fraction, or the friction between phases. So, designing high efficiency nozzles or even predicting their efficiency can be relatively complex. However, this is fundamental when designing the thermodynamic systems mentioned before. Nevertheless, the efficiency or even the outlet velocity is never considered in the literature dealing with flash nozzles CFD modeling.

Regarding the literature on flash nozzles, most of the early research studies were done on Loss of Coolant Accident (LOCA) nozzles. These studies were based on experimental and theoretical approaches [6]. One of the main goals was to predict the critical mass flow rate in case of rapid loss of coolant in nuclear plants. However, after the first two oil crises, increased interest in geothermal power and waste-heat energy recovery arose; using two-phase turbines looked promising in this context; consequently, various studies were conducted on two-phase turbine nozzles [2]. The prediction methods were based on 1D two-fluid approaches and on thermal phase change closure models as can be read in the work of Bussac [7].

The recent CFD methods mainly benefited the development or optimization of ejectors for transcritical CO_2 cycles. These methods are often derived from former 1D modeling approaches as can be read in [8]. As for the two-phase turbines, two-phase nozzles are also the motive elements of the ejectors and nozzle efficiency is a crucial parameter. However, in this sector, the entrainment ratio is studied at the expense of the nozzle efficiency [9].

Furthermore, literature on flash boiling in fuel injectors of IC engines exists. The research in that sector analyses in particular the impact of the early phase change on the shape of the fuel spray in the combustion chamber. The CFD analysis of Devassi on a fuel injection nozzle [10] is a typical example of the kind of studies conducted in this sector. Such studies are focused on mass flow rate and liquid jet shape prediction [11].

These works and others not cited here raised and tried to answer several questions. Particularly: What is the slip between liquid and gas? What should be the phase change formulation? At what pressure does the phase change start? How efficiently calibrate the models? An interesting discussion about these aspects is proposed by [12], a comprehensive literature survey on flash flows.

To the best knowledge of the authors, the nozzle efficiency prediction was not discussed in the cited or any other papers. So the present paper tends to fill this gap. It is done by a phase change models assessment focused on the ability of the models to reproduce the outlet flow conditions of experimental data from the literature. For this purpose, experimental test cases where nozzle outlet velocities were measured are used as reference.

Furthermore, a number of the papers cited above and many others are based on models that do not exploit the concept of interfacial area density; this is the case of the well known Homogeneous Relaxation Model (HRM) [13] used either for water or for CO_2 [8] and the case of models based on standard accommodation coefficients for mass sources [9]. Besides, other families of modeling strategies use the interfacial area density expression corresponding to the bubbly regime for nozzles where the void fraction could reach up to 0.7, like in the thermal phase-change modeling of [14] or the Hertz-Knudsen model (HK) based studies of [11]. Knowing that the bubbly regime is limited to void fractions below 0.3 [15], the interfacial area density formulation using this description is neither valid for the conditions mentioned above nor for two-phase turbines nozzles' since in that last case void fraction attains easily values up to 0.9 [16] which corresponds to a droplet regime situation.

To the best knowledge of the authors, the topology transition from a bubbly to a droplet regime was never before considered in literature dealing with flash nozzles CFD modeling. To fill this gap, a model never used before for such nozzles is explored in the paper. Indeed, when trying to calibrate the models on the mass flow and the outlet velocity simultaneously, the poor flexibility and difficulty of calibrating the models available in literature brought the author to explore a transitional interfacial area formulation that is a variant of the formulation proposed by Wu [15]. This modified model is also included in the model benchmark; it is named for the article ''non-symmetric Thermal-Bubble-Droplet'' (TA-BD) model.

In summary, this article deals with two aspects of two-phase nozzles modeling never treated before:

- The ability of literature phase change models to predict the nozzle efficiency in conjunction with the flow rate
- The exploration of a new variant of a transitional interfacial area formulation that aims to highlight the importance of this parameter in expanding flash flows especially when trying to predict the efficiency

The detail of literature models and their pros and cons are discussed in section 2.1.2.

The improved knowledge on CFD flashing flow modeling could improve the shape optimization techniques aiming to design more efficient components and systems. For this purpose, two nozzles were studied to evaluate the effect of the nozzle shape on the models' behavior.

The article is structured as follows. In section 2, the general equations treated by the multiphase CFD solver are presented. From this generality, the specificities and simplifications done by different models in the literature are introduced. The main phase-change mass transfer models of literature are discussed before the TA-BD model is presented. Subsequently, test cases based on two nozzle geometries are presented. Then in section 3 the simulation results and the models comparison are presented. The comparison is focused on the robustness and the ability of models to be calibrated regarding the mass flow rate and the outlet velocity that defines the nozzle isentropic efficiency.

2. Methodology

2.1. Constitutive equations

2.1.1. Conservation equations formulation

The general formulation of conservation equations for a two phase flow requires a phase per phase description. In the commercial CFD code Ansys CFX 16.0 these equations, describing the so called Euler-Euler model, are described by equations 1 to 4 for liquid. The same kind of equations is used for liquid and gas; index 1 is used for the liquid and 2 for the gas.

Continuity equation:

$$\frac{\partial}{\partial t}(\alpha_1\rho_1) + \nabla\left(\alpha_1\rho_1\vec{U}_1\right) = \Gamma_{12} \tag{1}$$

where Γ_{12} is the volumetric mass flow rate transferred from liquid to vapor. And $\Gamma_{12} = -\Gamma_{21}$.

Momentum equation:

$$\frac{\partial}{\partial t}\left(\alpha_1\rho_1\vec{U}_1\right) + \nabla\left(\alpha_1\left(\rho_1\vec{U}_1\otimes\vec{U}_1\right)\right) = -\alpha_1\nabla p + \nabla\left(\alpha_1\mu_1\left(\nabla\vec{U}_1 + \left(\nabla\vec{U}_1\right)^T\right)\right) + \Gamma_{12}\vec{U}_i + \vec{M}_1 \tag{2}$$

The term $\Gamma_{12}\vec{U}_i$ is the momentum source produced by phase change. The term $\vec{M}_1$ contains the forces transferred from phase 2 to phase 1 i.e. the interfacial drag forces.

Total energy equation:

$$\frac{\partial}{\partial t}(\alpha_1\rho_1 h_1^t) - \alpha_1\frac{\partial P}{\partial t} + \nabla\left(\alpha_1\rho_1\vec{U}_1 h_1^t\right) = \nabla(\alpha_1\lambda_1\nabla T_1) + \alpha_1\nabla\left(\vec{U}_1\tau_1\right) + \Gamma_{12}h_i^t + \dot{q}_1 \tag{3}$$

where $\dot{q}_1$ is the interfacial heat transfer rate.

The interfacial transfer terms $\Gamma_{12}\vec{U}_i$ and $\Gamma_{12}\,h_i^t$ take into account the flux direction as follows:

$$\begin{matrix} if\ \Gamma_{12} < 0 \\ if\ \Gamma_{12} > 0 \end{matrix}\ \vec{U}_i = \begin{cases}\vec{U}_1 \\ \vec{U}_2\end{cases} and\ \ h_i^t = \begin{cases}h_1^t \\ h_2^t\end{cases} \tag{4}$$

The CFX solver solves also the volume continuity equation, or volume fraction transport equation, expression 5, usually introduced in multiphase problems. Thus, in the general case 6 (+1) equations are solved.

$$\sum_p \frac{1}{\rho_p}\left(\frac{\partial(\alpha_p\rho_p)}{\partial t} + \nabla\left(\alpha_p\rho_p\vec{U}_p\right)\right) = \sum_p \frac{\Gamma_{pp'}}{\rho_p} \tag{5}$$

The index p refers to the phase (1 or 2) and the index p' to the remaining phase (i.e. 2 or 1).

One can read in the literature dealing with flash nozzle flows that the general multiphase description presented above is often reduced to a simpler formulation, such as:

- Euler-Euler formulation: this is the general formulation including the 6 generic equations and the volume fraction transport equation (6+1) [14].
- Mixture formulation: in this case the continuity and energy equations are shared by both phases while the momentum equation can be completed by a phase slip velocity model. The volume fraction transport equation is also solved for vapor. One gets 3+1 or +2 equations model. One may refer to [17] for the exact formulation. A simplified description, especially for energy equation, can be read in [18].
- Homogeneous formulation: here the momentum equation is shared by two phases; velocities are identical. The energy equation can be shared or not. The original description of this formulation is given by Downar [13].

An additional assumption very often found in literature is that vapor phase is saturated.

We shall comment on these formulations. Regarding the momentum equation, it seems reasonable to assume that gas and liquid will accelerate to different degrees given their density disparity and being subject to the same axial pressure gradient along the nozzle. The question is then if the velocity difference between gas and liquid has any substantial effect on the behavior of the nozzle. According to Yixiang [12] it has an important effect on the vapor generation rate, possibly because it affects the interfacial heat transfer rate. From an entropic point of view, friction between phases is a loss of kinetic energy and consequently affects the flow pattern and the exit velocity.

Concerning the use of a unique energy equation, since vapor quality attains relatively low values in flash flow nozzles, solving an energy balance only for the liquid phase seems reasonable; a number of authors propose this simplification either in a HRM framework [13] or in thermal phase-change model situation [14]. This goes often with the assumption that the vapor is saturated.

A summary of the type of formulations used in various papers is presented in Table 1; it is not exhaustive but it represents the major research areas dealing with flashing flows and the more popular modeling approaches. In addition to the modeling aspects it shows the maximum outlet void fraction and the type of modeled geometry.

From this table some conclusion can be done:

- There is a substantial disparity in the interfacial transfer models; this point is treated in the next section
- Papers using interfacial area density variable (A_i) do not take into account the droplet regime, only bubbly regime (A_{i_b})
- The majority of references are based on mixture formulation showing the interest of exploring the possibilities offered by Euler-Euler formulation
- There is not a preferred model for turbulence

In the next section the most meaningful types of interfacial mass transfer models are presented.

Table 1 : summary of some flashing flow CFD modeling works

Ref.	General formulation	Evaporative potential	Interfacial area density	Specific models	Turbulence model	Max outlet void fraction	Geometry	Software
[19]	Mixture	ΔP	A_{i_b}	Slip velocity	k-w SST	0.7	BNL nozzle	Fluent
[18]	Mixture	$\sqrt{\Delta P/P}$ & ΔP		Slip velocity	k-w SST	0.95	CO2 ejector	Fluent
[20]	Mixture	$\sqrt{\Delta P/P}$			k-e	0.7	BNL nozzle	Fluent
[11]	Mixture homogenous	ΔP $\Delta \dot{x}$	N_b cte or f(T) d_b : cte		k-w SST	0.98	''Moby Dick'' nozzle	Fluent
[21]	Mixture homogenous	$\Delta \dot{x}$			Realizable k-e	...	CO2 ejector	Fluent
[22]	Mixture	ΔT	$\dot{N}_b$: Jones $A_{i_b} + A_{i_{slu}}$	N_b transport equation	k-e	0.7	BNL nozzle	CFX
[9]	Mixture homogenous	$\Delta T/T$			k-w SST	0.98	CO2 ejector primary nozzle	Fluent
[23]	Mixture	$\sqrt{\Delta P/P}$ & $\Delta T/T$		Slip velocity	Realizable k-e	0.95	R134a ejector primary nozzle	Fluent
[14]	Euler-Euler	ΔT	A_{i_b}		k-w SST	0.7	BNL nozzle	CFX
[10]	Mixture	ΔP	A_{i_b}; N_b f(T)			1	Fuel injector	AVL FIRE
[24]	Mixture	$\Delta \dot{x}$			RNG k-e	1	Fuel injector	CONVERGE

2.1.2.Interfacial transfer terms

In this section the mass, energy and momentum interfacial transfer models are presented.

2.1.2.1. Interfacial mass transfer

The mass transfer models are rather diverse. The authors tried here to get a global vision of this diversity and propose a classification in order to emphasize their main characteristics.

The general formulation of the mass transfer from liquid phase to vapor phase is based on a potential (ϕ) and on what we will call a relaxation term (K).

$$\Gamma \propto K\,\phi \tag{6}$$

The potential represents the distance from a thermodynamic equilibrium. The metastability is an image of this distance to the equilibrium. The greater this distance the greater the mass transfer. This is why a metastable situation is intended to disappear. The relaxation coefficient represents the relation between the potential and the mass flow; it takes several forms. Here, the models are classified by types of potential. Regarding the relaxation terms, only a selection of some formulations used for model comparison is presented here. Also a specific sub-section for the interfacial area density is presented at the end of the section.

2.1.2.1.1. Pressure difference based models

The mass flow potential can be computed as the difference between the saturation pressure and the actual static pressure. The saturation pressure is a function of the liquid or mixture temperature. This potential was extensively used in modeling of cavitating flows. The reference model is the Singhal model which is based on Rayleigh-Plesset bubble growth analysis [25]. It was also used for depressurized flows [20]. The reader may refer to Singhal's work [25] for more details. To the best knowledge of the author, the Singhal formulation is only used for moderate average void fraction flows (< 0.5). The average void fraction here refers to the same of the Table 1 i.e. the cross sectional device average.

For flows dealing with high void fractions, the Hertz-Knudsen (HK) formulation is used. That is the case in the work of Karathanassis [11]and Le [19] on water nozzles or Yazdani [18] for CO2 two phase ejectors.

The general expression of the mass flux is based on the kinetic theory of gases and it is named Hertz-Knudsen relation:

$$\Gamma = K_{\Delta P}\,(P_{cavit}(T) - P) \tag{7}$$

The relaxation term can take a multitude of forms but the basic relation for $K_{\Delta P}$ takes the following form:

$$K_{\Delta P} = \lambda_{\mathrm{acc}}\,\alpha_l\,\rho_l \tag{8}$$

where λ_{acc} is an accommodation coefficient, α_l the liquid volume fraction and , ρ_l the liquid density. A multitude of variants of this relaxation terms were used by different authors. An interesting benchmark study was done by Karathanassis [11]; he observed that for high temperature water flashing flows equation 9 seems to give reasonable results compared to experimental data. It is based on pressure difference potential and an accommodation coefficient as described in equation 9 and a constant interfacial area density ($\mathrm{A_i}$) defined in equation 10.

$$K_{\Delta P\_K1} = \frac{\lambda_{\mathrm{acc}}\mathrm{A_i}}{\sqrt{2\pi \mathrm{R_g T_{int}}}} \tag{9}$$

$$\mathrm{A_i} = 4\,\pi\,(\mathrm{d_b}/2)^2\mathrm{N_b} \tag{10}$$

The value of $\mathrm{N_b}$ was 10^{13} 1/m^3 and the bubble diameter was 10^{-6}m in the cited paper. These values will be used for the computations presented in this paper.

The interface temperature $\mathrm{T_{int}}$ was assumed to be equal to the local cell temperature.

The reference pressure was called the cavitation pressure and was expressed as follows [17]:

$$P_{cavit} = P_{sat}(T) + 0.195\,\rho_{mix}\,k_T \tag{11}$$

where k_T is the turbulent kinetic energy and ρ_{mix} the mixture density. This expression is supposed to capture the effect of turbulence on cavitation onset. Note that this expression was originally included in the Singhal model.

The conservation equations in Karathanassis were written in a mixture formulation frame work without slip between phases. The details of formulations, especially for energy, can be found in Ansys Fluent user's guide [17] or in various articles of which a good example is [26].

2.1.2.1.2. Vapor quality difference based model

The potential driving the mass transfer can be expressed as the difference between the thermal equilibrium quality and the actual quality. This approach was proposed by Downar [13] and reused by Karathanassis [11] for water flash flow nozzles, by Lorenzo [27] for transient water flash flows, and by Palacz [21] for a CO_2 ejector.

It is called Homogeneous Relaxation Model (HRM) and its general form is:

$$\Gamma = \frac{\rho}{\Theta}(\bar{x}(P) - x) \tag{12}$$

where $\bar{x}$ is the equilibrium vapor quality and Θ a relaxation time. It was named "homogeneous" because the two phases were supposed to have the same velocity even if they were not sharing the same temperature. Downar [13] expressed the equilibrium quality as follows:

$$\bar{x} = \frac{h_{mix}(P,x) - h_{sl}(P)}{h_{sg}(P) - h_{sl}(P)} \quad (13)$$

where the mixture enthalpy is:

$$h_{mix} = x\, h_{sg}(P) + (1-x) h_{ml} \quad (14)$$

The authors [13] call h_{ml} metastable liquid enthalpy; since the mass transfer does not affect the energy equation they used (same for [21]), it seems to correspond to inlet liquid enthalpy. However, one can read in [28] that liquid enthalpy may change during expansion for HRM model; that requires including a source term in the liquid energy balance and so was done for the present work.

Then the final form of the mass flux is given by Downar et al. [13]:

$$\Gamma = \frac{\rho}{\Theta}(1-x)\frac{h_{ml} - h_{sl}(P)}{h_{sg}(P) - h_{sl}(P)} \quad (15)$$

The relaxation time Θ is defined by semi-empirical correlations presented in Downar-Zapolski et al. [13] :

$$\Theta = \Theta_0 \alpha^a \psi^b \quad (16)$$

Here ψ is a non dimensional pressure difference; for pressures lower than 10bar it is defined as:

$$\psi = \left| \frac{P_{sat}(T_{in}) - P}{P_{sat}(T_{in})} \right| \quad (17)$$

For higher pressures this is defined as follows:

$$\psi = \left| \frac{P_{sat}(T_{in}) - P}{P_{crit} - P_{sat}(T_{in})} \right| \quad (18)$$

The exponents in equation 16 are fitting coefficients. The recommended values for low and high pressures, in the case of water, are presented in Table 2.

Table 2 : HRM model empirical constants

$P < 10bar$	$P > 10bar$
$\Theta_0 = 6.51\,.10^{-4}\ s$	$\Theta_0 = 3.84\,.10^{-7}\ s$
$a = -0.257$	$a = -0.54$
$b = -2.24$	$b = -1.76$

Note that α and ψ are both increasing functions when approaching the outlet of the nozzle. Thus, they should produce a similar effect on relaxation time. Also the expression of the equilibrium quality (eq. 13) is questionable: the vapor quality is computed from an enthalpy which should be the equilibrium enthalpy (isentropic or isenthalpic) but it is computed with what seems to be the mixture's meta-stable enthalpy. Nevertheless the HRM model uses 3 tuning parameters and should therefore have sufficient degrees of freedom for calibration. This ability will be called flexibility in the next sections.

2.1.2.1.3. Temperature difference based model

The potential associated with the non-equilibrium can also be expressed as the difference between the saturation temperature ($T_{sat}(P)$), function of the static pressure, and the liquid temperature (T_{liq}).

The most notable model based on this difference is the so called thermal phase change model. The basic idea is to compute the heat flux associated with the phase change when mass transfer occurs. The mass flux is:

$$\Gamma = \frac{\dot{q}_i}{\Delta h_{gl}^t} = \frac{h_i\, A_i}{\Delta h_{gl}^t(P)} (T_{sat}(P) - T_l) \quad (19)$$

where h_i is the interfacial heat transfer coefficient, A_i is the interfacial area density (in m²/m3) and Δh_{gl}^t is the total enthalpy difference between the gas and liquid. The interfacial heat flux ($\dot{q}_i$) is applied also to the energy balance. This expression shows the relation between the capacity of the fluid to internally transfer heat from liquid to vapor and its ability to change phase.

This formulation was used by Wu [15] and Yixiang [14] who worked on two phase nozzle flows mostly for nuclear power plant safety issues or in the work of Bussac [7] who worked of two phase impulse turbines. One of the main goals was to predict the mass flow rate of the nozzles.

Regarding the heat transfer coefficient, Yixiang [14] proposes to use the Aleksandrov heat transfer coefficient that was derived from bubble growth analysis in superheated liquids [29] to take into account the gas/liquid velocity difference through the Péclet number.

$$h_c = \frac{\lambda_l}{l_c}\left(\frac{12}{\pi^2}Ja^2 + \frac{1}{3\pi}Pe\right)^{1/2} \quad (20)$$

where λ_L is the liquid's thermal conductivity and l is the interfacial characteristic length; in the case of bubbly flow, this is the bubble diameter. The Jakob number is:

$$Ja = \frac{C_p \rho_l (T_l - T_{sat})}{\rho_g \, \Delta h_{gl}^t} \quad (21)$$

where C_p and ΔH_{gl} are respectively the isobaric heat capacity, and the latent heat of the liquid. The Péclet number is:

$$Pe = \frac{\left|\vec{U}_g - \vec{U}_l\right| l_c}{D_{T,l}} \quad (22)$$

where $D_{T,l}$ is the thermal diffusivity of liquid. In the cited Yixiang model, the heat transfer coefficient is multiplied by a correction factor k_h in order to add a calibration parameter to the formulation.

We could also cite in this section the work of Giacomelli [9] and Geng [23] who use a dimensionless temperature difference for a CO_2 and R134a two-phase ejector primary nozzle modeling. They used the $K_{\Delta P}$ term of equation 7 multiplied by $(T_{sat} - T)/T_{sat}$.

The interfacial area density A_i, that can be used in ΔP and ΔT based models, is an essential parameter of the multiphase flow behavior. That is why a specific section is attributed to it in this paper.

2.1.2.1.4. Interfacial area density

The treatment of the interfacial area density (A_i in equations 9, 19 and 30) needs to rely on several assumptions if one wants to avoid to use detailed interface tracking techniques. A solution proposed by some authors is to model the transport and source terms of variables associated with interfacial area. This is the case of the MUSIG (multiple size group [30]) model that resolves the momentum equation for the dispersed phase using an Euler-Euler flow description. It is based on a bubble population balance equation. This model has evolved later to introduce the transition to the continuous gas phase (GENTOP model [31]) in an attempt to obtain a general model. The difficulty these methods try to address is the treatment of the diversity of characteristic sizes and velocities describing a multiphase flow. It requires additional transport equations (one per sub-size fraction for inhomogeneous MUSIG model) and a variety of models for shape transition, coalescence or breakup source terms, etc. Nevertheless the generalization remains hard to achieve as can be concluded from the simulation configuration of those models [31].

A simpler approach consists in proposing a relation between the void fraction and the interfacial area density. Wu [15] defines it for the first stage of phase change ($\alpha < 0.3$) as an increasing function of the void fraction and the number of bubbles per unit volume (N_b) Assuming equal sized spherical bubbles, Wu writes:

$$A_{i_b} = (6\alpha)^{2/3}(\pi \, N_b)^{1/3} \quad (23)$$

The value of the bubbles number was assumed to be constant by Wu. Maksic [22] proposed to use a bubble transport equation including a volumetric nucleation rate based on Jones model.

When the void fraction increases, the bubbly flow should evolve to a bubbly-slug flow for which Wu gives an approximation based on a Taylor bubbles description:

$$A_{i_{slu}} = (4\alpha_T)^{\frac{2}{3}}/(\alpha_{max}^{1/6} D) \quad (24)$$

where D is the channel diameter and α_T is the Taylor bubbles void fraction. This second expression was used, added to A_{i_b} (equation 23), by Maksic to compute the final interfacial are density ($A_{i_b} + A_{i_{sl}}$) [22] with a maximum void fraction (α_{max}) of 0.8. No precision about how to get α_T was given by Maksic. Yixiang used A_{i_b} for void fractions lower than 0.7 in a converging diverging nozzle [14]; in Yixiang's paper, the particle model is mentioned. This seems to refer to the CFX particle model [32] in which A_{i_b} is based on a clipped void fraction ($\tilde{\alpha}$) for high void fractions (α >0.8) in order to decease A_{i_b} when approaching unit void fraction; this clipping was implemented for the present paper as well.

$$\tilde{\alpha} = \begin{cases} \max(\alpha, \alpha_{min}) & if(\alpha < \alpha_{max}) \\ \max\left(\dfrac{1-\alpha}{1-\alpha_{max}}\alpha_{max}, \alpha_{min}\right) & if(\alpha \geq \alpha_{max}) \end{cases} \quad (25)$$

For void fractions higher than 0.7, according to Wu, the flow is considered as being mist flow. The term ''mist flow'' refers, in gas-liquid flow analysis, to a regime where the disperse phase (liquid droplets) is transported by the gas phase. In these conditions, the interfacial area density for constant sized droplets is:

$$A_{i_d} = (6(1-\alpha))^{2/3}(\pi\, N_d)^{1/3} \quad (26)$$

The number of droplets per unit volume (N_d) was assumed to be equal to N_b by Wu. Wu proposed a symmetric model assuming that transition from bubble to droplet regime is done at constant area density from 0.3 to 0.7 void fractions.

With an idea similar to the ones of Maksic or Jones, Karathanassis proposed to use a non constant N_b (equation 27). He referred to a work dealing with flash boiling sprays in which the authors localized the bubble formation in the initial stage of the flash process and wrote that the nucleation depends on the degree of superheat of spray corresponding to the injection back pressure at the inlet temperature [33]. It is not clear how this was implemented in Karathanassis' simulation but it seems that N_b was computed for every axial location. Otherwise he tested a constant value of A_i.

$$N_b = 10^{13}\exp(-5.28/\Delta T_{sup}) \quad (27)$$

Devassi [10] used the same superheat based formulation also for N_b ; he computed it for every point in the flow. However since the inlet is in a sub-cooled state, inlet superheat is negative so when going through the expansion, superheating goes through zero and N_b through infinite; so this formulation is not adapted for motive nozzles.

In the present work a non-symmetric bubble to droplet transition model was tested. To the knowledge of the author, this is the first time this is implemented and analyzed in any depressurizing two phase flow analysis.

The interfacial area density will be modeled by a simple linear interpolation between the maximum bubble regime A_i and the maximum droplet regime A_i. This leads to the general formulation expressed by equation 28.

$$A_i = \begin{cases} if\ \alpha \le \alpha_b : (6\alpha)^{2/3}(\pi\, N_b)^{1/3} \rightarrow A_{ib}\ (bubbly\ regime) \\ if\ \alpha \ge \alpha_d : (6(1-\alpha))^{2/3}(\pi\, N_d)^{1/3} \rightarrow A_{id}\ (droplet\ regime) \\ else : linear\ interp\ A_{ib}|_{\alpha_b}\ to\ A_{id}|_{\alpha_d}\ (transition) \end{cases} \quad (28)$$

The values for the transition void fractions were proposed by Wu et al. [15]. These values could be subject to a parametric study, but were supposed to be $\alpha_b = 0.3$ and $\alpha_d = 0.7$. In contrast to the Wu model, this model does not state for which regime (bubble or droplet) the maximum A_i is observed and does not assume a constant $A_i$between the two regimes.

In Ansys-CFX, for Euler-Euler problems composed of two continuous phases, the interfacial area density is expressed as follows:

$$A_i = \frac{\alpha(1-\alpha)}{l_c} \quad (29)$$

Please note that in the CFX GUI and theory guide, an Euler-Euler model composed of two continuous phases is named ''mixture'' model. From an implementation point of view, the interfacial length scale l_c has to be given by the user either as a constant either with a CEL expression; so in this work l_c was expressed as a function of α and $\mathrm{A_i}$ ($l_c = \frac{\alpha(1-\alpha)}{\mathrm{A_i}}$ Ai from equation 28).

In order to avoid getting non defined values of l_c at α values of 0 and 1, the volume fraction is capped to a certain minimum value; a value of 1e-7 was taken for this work. Note that liquid volume fraction is $(1-\alpha)$ and A_{i_b} and A_{i_d} are null at 0 and 1 void fraction respectively. An example of transitional interfacial area density is given by Figure 4. The part of the curb starting at $\alpha = 0$ is A_{i_b} and the part at high values of α corresponds to A_{i_d}.

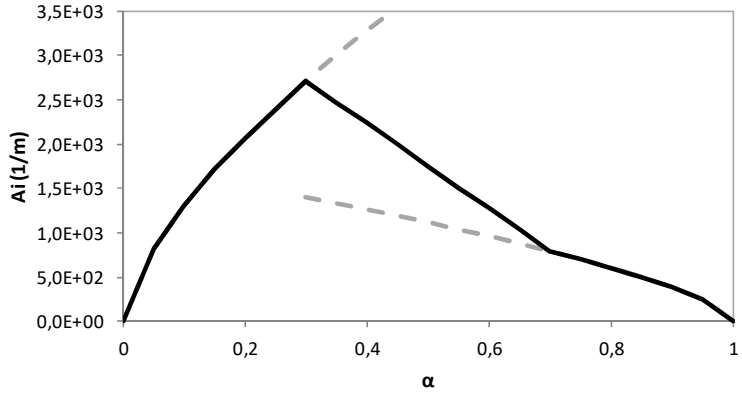

Figure 4 : non symmetric interfacial area density example $N_b = 2.10^9$ and $N_d = 5.10^7$

2.1.2.2. Momentum transfer

The interface momentum transfer term ($\vec{M}_{12}$ in equation 2), includes the drag force between liquid and gas. It has the following form [17]:

$$\overrightarrow{D_I} = \frac{C_D}{8} A_i \, \rho_l \left(\overrightarrow{U_2} - \overrightarrow{U_1}\right) \left|\overrightarrow{U_2} - \overrightarrow{U_1}\right| \quad (30)$$

No other interfacial forces were modeled here and thus $\vec{M}_{12} = \overrightarrow{D_I}$.

The first simulations done for this paper were done using TA-B model [14] where the drag force model is the one of Ishhii-Zuber which includes the effect of gravity. Some tests were done during the actual research work using Schiller-Neumann [17] and constant drag coefficient models and no significant differences were found, notably, the Schiller-Neumann model computed a constant value of 0.44 in the entire diverging section of the nozzle. That is why in the models computing liquid and gas velocities separately, equation 30 in conjunction with a constant C_D value was used.

2.2. Test cases

One of the intentions of this paper is to discuss the advantages of modeling the transition from bubbles to droplets in the interfacial area density formulation when trying to predict the nozzle behavior and efficiency in particular. The bubble and droplet numbers may depend on several parameters, that is why we selected test cases with different inlet/outlet conditions and geometries. Two nozzle geometries were tested in order to explore the effects of nozzle shape of the models.

2.2.1. Ohta B nozzle

In the early 90's, a Japanese team [16] worked on waste heat recovery by impulse turbines using phase change nozzles. Two nozzle geometries were tested. The first was called B nozzle which is a fairly simple nozzle. It was widely studied for a wide outlet pressure range. The authors measured mass flow rate, efficiency and pressure profiles. The efficiency was obtained thanks to thrust measurements. The dimensions and the operating conditions are shown in Figure 5 and Table 3 respectively.

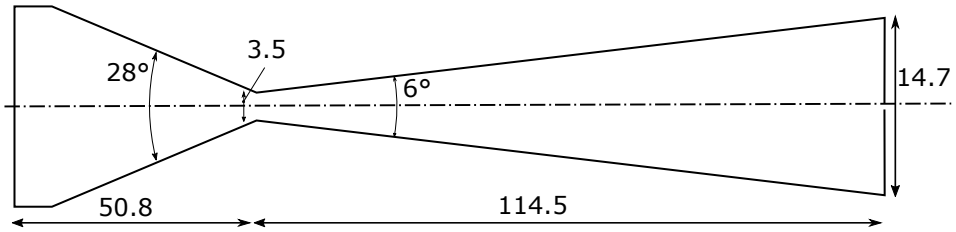

Figure 5 : Ohta B nozzle

Table 3 : Ohta B nozzle operating points

$T_{in}(°C)$	$P_{in}(kPa)$	$SC(K)$	$P_{out}(kPa)$	$\dot{m}(g/s)$	Ref.
148	470	1,5	18/45/73/100	122	[16]
137,5	470	12	16/43/70/100	156	[16]

The range of operating sub-cooling degrees (SC), inlet temperatures and outlet pressures are particularly useful for the purposes of this article. Note that the mass flow in Table 3 does not depend on the outlet pressure; that means that the nozzle operates in critical conditions.

2.2.2. Ohta F nozzle

The Ohta team tested a second nozzle with a long throat called F nozzle; the goal was to increase the cavitation inception pressure and thus the efficiency of the nozzle. The authors made mass flow, efficiency and pressure profile measurements as well. The tested operating conditions and geometry are presented bellow.

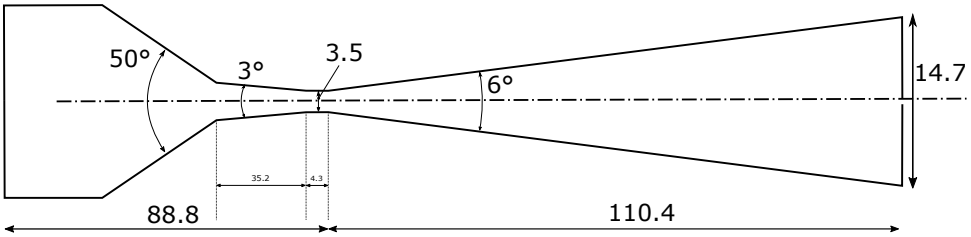

Figure 6 : Ohta F nozzle

Table 4 : Ohta F nozzle operating points

$T_{in}(°C)$	$P_{in}(kPa)$	$SC(K)$	$P_{out}(kPa)$	$\dot{m}(g/s)$	Ref.
148	470	1,5	20/47/74/100	118	[16]

Operating conditions are given in the Table 4. This case allows us to test the validity of the interfacial area formulation for a different section variation.

The uncertainties of the measured data reported in [16] are within 2% for mass flow rate, 2% for thrust, 1% for pressure and 0.5% for temperature. This leads to an uncertainty of 2.8% for velocity by uncertainty propagation (knowing that thrust is equal to $\dot{m}.V$) and thus around 5% for efficiency.

3. Results and discussion

In this section the configuration of the CFD solver, a summary of the physical formulation, a mesh sensitivity test and test results for the 3 nozzles are presented.

3.1. Configuration and models

Four different models were implemented regarding the governing equations and interfacial mass transfer formulation. The first three are based on models from literature which represent the main families of methods to model the flow and mass transfer phenomena in two phase nozzles. The last one is a variation of one of them. A summary of the four formulations is given here:

- HK model based on [11]: mass, momentum and energy conservation equations are shared by both phases. Mass transfer is computed using equations 7 and 9. Please refer to [11] and [18] for details on governing phase hydrodynamic equations. The main physical characteristics of this model are: no slip between phases, same energy equation, constant interfacial area density and the use of only one calibration parameter.
- HRM model based on [13]: mass and momentum conservation equations are shared by both phases. Energy equation is solved only for liquid. Vapor is assumed to be in saturated condition. Mass transfer is computed using equations 15 to 17. The main physical characteristics of this model are: no slip between phases, saturated vapor, and the use of three calibration parameters.
- TA-B model based on [14]: Euler-Euler model assuming saturated vapor. Interfacial drag coefficient equal to 0.45. Mass transfer is computed using equations 19, 20 and 23. The main physical characteristics of this model are: different phase velocities, saturated vapor, and the use of two calibration parameters.
- TA-DB model: Euler-Euler model assuming saturated vapor. Interfacial drag coefficient equal to 0.45. Mass transfer is computed using equations 19, 20 and 28. The main physical characteristics of this model are: different phase velocities, saturated vapor, and the use of two calibration parameters.

The nozzles had as boundary conditions static pressures, temperature and void fraction at inlet and static pressure at outlet. The inlet void fraction was set equal to 1 for liquid. The wall was configured with default parameters (no slip wall). The nozzle flow was supposed to be axisymmetric. A 3° revolution form was therefore used to model the control volume with two symmetry planes as its limits.

Regarding the state of the fluids, the liquid properties (ρ, C_p, μ) were computed as a function of temperature computed from the enthalpy resulting from the energy balance which means that the liquid's meta-stable condition was computed by considering it in a temperature based saturation state and not in a pressure based saturation state. The vapor was supposed to be in pressure based saturated conditions i.e. its properties were function of the static pressure.

The liquid and vapor properties of water were computed from standard IAPWS IF97 tables available in Ansys CFX. The flow is turbulent; the Reynolds number at the outlet is around 30.10^3 and around 130.10^3 close to the throat. The kwSST closure was used as turbulence model since this is the one preferred for adverse pressure gradient flows that could happen for some operating conditions [17]. One of the advantages of the kwSST model is its ability to switch from a low-Reynolds boundary layer treatment to a standard boundary layer treatment.

The CFX solver is a coupled solver using a pseudo-transient formulation; the coupled option was selected for volume fraction as well. A bounded second-order upwind scheme was selected for advection. Please refer to Ansys CFX [32] documentation for details on numerical resolution.

A steady state simulation was done. The physical time step was set in a range between 1.10^{-4} s and 1.10^{-8}s depending on the mesh size and the model. This parameter acts like a relaxation coefficient. The simulation was supposed converged when the mass and energy imbalance was lower than 0.5%, the inlet mass flow rate was steady and the outlet velocity was steady; all residuals were in this situation lower than 1.10^{-5}. The total energy formulation of the energy conservation equation was selected. The flow field was initialized at 0 vapor volume fraction, at inlet temperature and pressure and at 0m/s velocity.

3.2. Mesh sensitivity

In order to maximize the quality within reasonable computational times, a mesh sensitivity analysis was done. The mesh was composed by prisms at the symmetry axis and hexahedrons everywhere else.

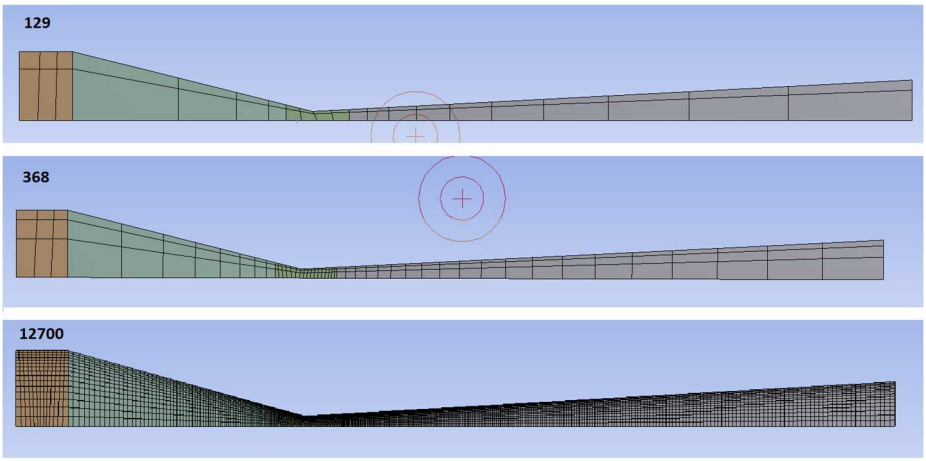

Figure 7 : 3 mesh examples with corresponding number of nodes

During this work it was observed that convergence is improved when several control volumes are used axially dividing the nozzle into several parts; this is certainly related to mesh interface control sections added by this operation. The corresponding mesh parts can be seen in Figure 7. In this same figure, 3 mesh examples are illustrated; the number in the left top corner is the number of nodes.

The tested case is the Ohta B nozzle at inlet condition of 1K sub cooling and two different outlet pressures: 100kPa and 45kPa. The TA-BD model was used with the parameters of Table 6.

The results were monitored in terms of mass flow rate and outlet velocity. The effect of mesh was quantified comparing the results to those of the more dense mesh. The mass flow difference is shown in Figure 8 and the outlet velocity difference in Figure 9. Note that for each calculation the case was reinitialized.

The maximum difference to the more dense case was about 2% for both outlet pressures and monitored parameters.

For the lighter mesh, the Y+ values were ranging between 100 and 1000, and for the more dense mesh between 10 and 20. Yixiang [14] obtained similar Y+ values for BNL flash nozzle simulations and the results were relatively well in agreement with experimental observations. That suggests that standard wall treatment is quite sufficient to model the dominating physical phenomena of flash boiling in such nozzles.

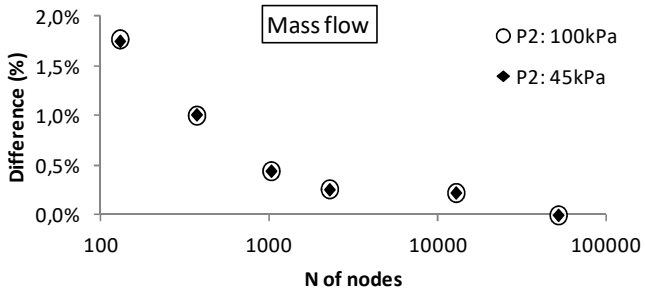

Figure 8 : difference with the more dense mesh; mass flow

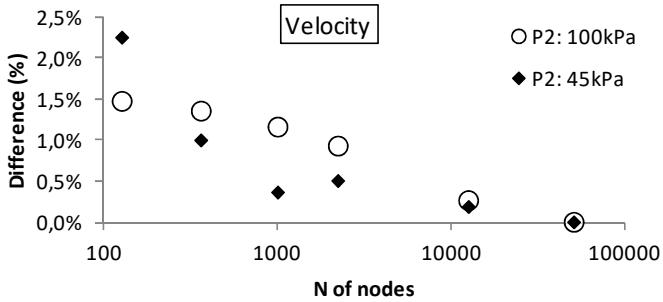

Figure 9 : difference with the more dense mesh; velocity

The mesh used for simulations was consisted of 12700 nodes, resulting from 15 radial subdivisions and a 2.10^{-4} m of axial mesh size in the central part of the control volume.

For nozzle F nozzle the same number of cells per unit volume was used with similar boundary layer mesh sizes.

3.3. Test cases

In this section the method by which the models were calibrated and tested are presented followed by the comparisons to the experimental results. The CFD results are compared in terms of mean mixture velocity, wall static pressure, inlet mass flow rate or efficiency. The latter is defined as follows:

$$\eta = \frac{V_{\overline{gl}}^2}{V_m^2} \tag{31}$$

This shows the importance of good outlet velocity prediction for nozzle efficiency computation; velocity discrepancies are amplified by the power applied to $V_{\overline{gl}}$.

The mean velocity is computed as follows:

$$V_{\overline{gl}} = x\, V_g + (1-x) V_l \tag{32}$$

Please note that for models using a unique momentum equation one get's $V_g = V_l$ (models HK and HRM).

The maximum velocity is the isentropic velocity:

$$V_m = \sqrt{2\left(h_{out\_s}(P_{out}, s_{in}) - h_{in}(P_{in}, T_{in})\right)} \tag{33}$$

For the models' accuracy comparison, a mean error is given for the available variables (φ); it is computed as follows:

$$er_\varphi = \frac{1}{n}\sum \frac{|\varphi_{CFD} - \varphi_{REF}|}{\varphi_{REF}} \tag{34}$$

where n is the number of measured points. When the error refers to pressure or void fraction profile, the value of φ_{CFD} is obtained by interpolation at a given axial position. In the case of a mass flow result comparison, the non absolute relative error is given.

3.3.1. Calibration and test process

The general procedure to calibrate and test the CFD models was to:

- get a mass flow rate close to the experimental one
- Try to get the nozzle outlet velocity for one of the outlet pressures. This is a crucial step when evaluating the ability of models to be calibrated. This is done for the highest outlet pressure. The calibration was assumed as achieved when discrepancy was lower than 1% for both mass flow rate and velocity at the pressure considered. When velocity calibration appeared as incompatible with flow rate calibration, the parameters adapted for the correct flow rate were maintained. At the end of this step the empirical constants of the model are assumed to be calibrated.
- Test the model on the three other outlet pressures using the calibrated parameters in order to observe the robustness of the models to changes in outlet pressure. If models react correctly when changing outlet pressure that means that one outlet pressure point is sufficient for calibration.

Models' parameters variation for calibration was done by trial and error approach using as departure point the parameter values from reference papers.

Besides, note that the flow rate is not dependent on the outlet pressure but varies with the degree of sub cooling; thus the first calibration step can be repeated when the sub-cooling changes in order to maintain a good precision.

We recall the calibration parameters for the 4 tested models: for the HK model, the adaptation parameter λ was tuned, for the TA-B model one can tune N_b and k_h parameters, for the HRM model the parameters ''Θ_0'', ''a'' and ''b'' can be modified, and for the TA-BD model N_b and N_d are tuned.

3.3.2. Ohta B nozzle

This nozzle was experimentally characterized in terms of mass flow, outlet velocity and static pressure profiles for two inlet sub-cooling degrees.

3.3.2.1. 1.5K sub cooling

3.3.2.1.1. Results summary

After the first calibration step, the mass flow rate obtained by all the models was of 122g/s with less than 1% error. However, when trying to obtain the measured outlet velocity only the TA-BD and HRM models could be effectively calibrated. The values of calibration parameters are given in the Table 5.

Table 5 : calibrated parameters; Ohta B 1K

λ (HK)	Θ_0/a/b (HRM)	N_b/k_h (TA-B)	N_b/N_d (TA-BD)
$2{,}4\,.\,10^{-2}$	$1{,}45\,.\,10^{-4}/-0{,}26/-1{,}75$	$1\,.\,10^{9}/\,8$	$3.5\,.\,10^{10}/1.85\,.\,10^{9}$

The velocities for the 4 outlet pressures are shown in Figure 10. One can check the outlet velocity at 100kPa outlet pressure for different models; the points for the HRM model and for TA-BD model are superposed on the measured value. The value for HK model is very close to the measured value, but getting a more accurate velocity is not possible when the target mass flow rate is obtained. In the same figure, in the case of TA-BD model, the velocities for other pressures show that when pressure is reduced, the model reproduces very well the measurements.

The nozzle efficiency chart shown in Figure 11, shows that all models can capture the efficiency dependence on the pressure as measured by Ohta. Nevertheless efficiency discrepancies are relatively important for the 3 literature models at optimal efficiency pressure (45kPa); for the TA-BD model it is lower than 1% while for the HRM model the discrepancy on maximal efficiency is 18%.

These 4 models could be used for optimal outlet pressure research. But the most representative model is the TA-BD model at least for these operating conditions. This suggests a better adaptation of this model to high expansion ratios. No obvious reasons for this difference to other models was found but the absence of the pressure directly in the source term and the specific formulation of Ai are probably a part of the explanation.

Regarding the pressure profiles on Figure 12 close to the nozzle outlet, the TA-B and TA-BD models are most accurate. The HK and HRM models produced a shock wave close to the outlet; this seems to be related to an over estimation of the velocity before the chock. These two models use a unique momentum equation so it could be related to the absence of velocity slip between phases.

At the throat HRM, TA-BD and especially the TA-B model show a pressure plateau; this is related to a vapor pocket located just after the throat and absent in the HK model results.

Regarding the average errors, the best models are the TA-BD and HRM models. Average errors on outlet velocity, pressure mass flow rate are reported in the Table 6.

Table 6 : summary of errors; Ohta B 1K

	TA-BD	HRM	TA-B	HK
er_V	0,7%	6,9%	12%	12%
er_P	9%	17%	13%	15%
$er_{\dot{m}}$	<1%	<1%	<1%	<1%

The TA-BD model is the most robust i.e. it is the one presenting the lowest average error when changing outlet pressure. This is particularly interesting in the perspective of two-phase ejector simulations where the mixing pressure i.e. the outlet pressure of the primary flow, is not known a priori.

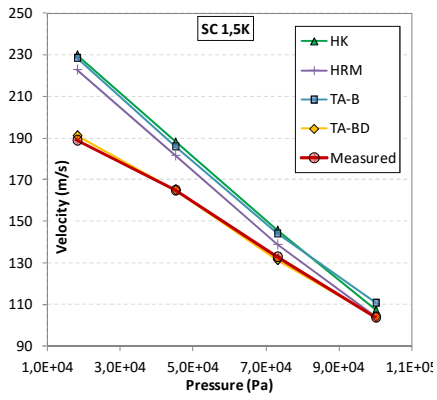

Figure 10 : outlet velocity function of outlet pressure; SC1.5K;nozzle B

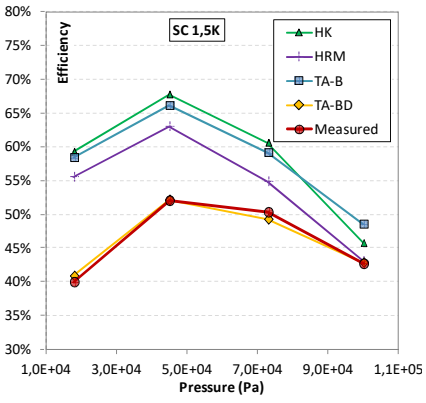

Figure 11: nozzle efficiency function of outlet pressure; SC1.5K;nozzle B

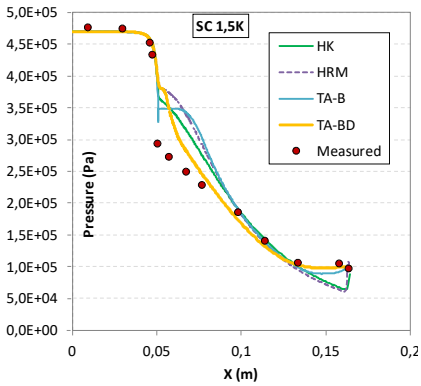

Figure 12 : static pressure profiles; SC1.5K 1bar outlet pressure; nozzle B

3.3.2.1.2. About calibration and flexibility of models

The two calibration objectives were the measured mass flow rate and the outlet velocity for 100kPa outlet pressure. During calibration process a certain number of flow rate and velocity couples were obtained; they are shown in Figure 13; the values were divided by the corresponding reference flow rate or velocity which results in a non dimensional plot. The resulting non-dimensional velocity was called velocity coefficient and the non-dimensional pressure is called pressure coefficient. The closer those coefficients are to unit, the better is the matching with experiments. This plot represents a space of solutions and helps during the calibration procedure; also it shows the limited space of possible solutions for some models.

For the HK model the adaptation coefficient was modified. An increase in λ produces a flow rate reduction and an outlet velocity increase. A unique $(\dot{m}/V)$ fraction is possible; this results on a line of solutions on the solutions space (triangles in Figure 13). The figure shows the case at 1bar outlet pressure; for this specific case, the predicted velocity is close to the measured one at the target mass flow rate, but if this procedure has been done for another outlet pressure, the target point would have been far from the solutions line (see velocity values in Figure 10).

The TA-B model includes N_b and k_h as parameters. The former was tested from 8.10^8 to 1.10^{12} and 3 values were tested for the latter: 1, 8 and 16. The resulting purple points were obtained in Figure 13. Increasing N_b or k_h has a similar effect to increasing λ; this can be easily understood looking to transfer equations. This leads to a narrow band of $(\dot{m}\ ;\ V)$ couples of the TA-B model solutions.

The HRM model's parameter Θ_0 was tested between 1.10^{-4} and 20.10^{-4}. Regarding ''a'' and ''b'', a preliminary analysis showed that both have a similar effect on the results (see comments on HRM model regarding α and ψ) but changing ''a'' produces less effects than changing ''b''. For example increasing ''a'' and ''b'' of 10% produce an increase of the mass transfer of +4% and +25% respectively.

At the end the parameter ''a'' was maintained at its original value of -0.257 and ''b'' was varied between -0.9 and -2.24. The resulting red points were obtained. The reduction of $''\Theta_0''$ and increase of ''b'' tend to increase the velocity and reduce the flow rate. Nevertheless the coupling between $''\Theta_0''$ and ''b'' was high and the responses far from linear making calibration laborious. However, the flexibility of this model is good and results in a large space of solutions in Figure 13. Thus, both the target mass flow rate and the outlet velocity could be obtained.

The calibration process of the HRM model is quite difficult since the parameters are strongly coupled and the associated effects are non linear; that explains why specific calibration techniques were developed for HRM using genetic algorithms by some authors [8].

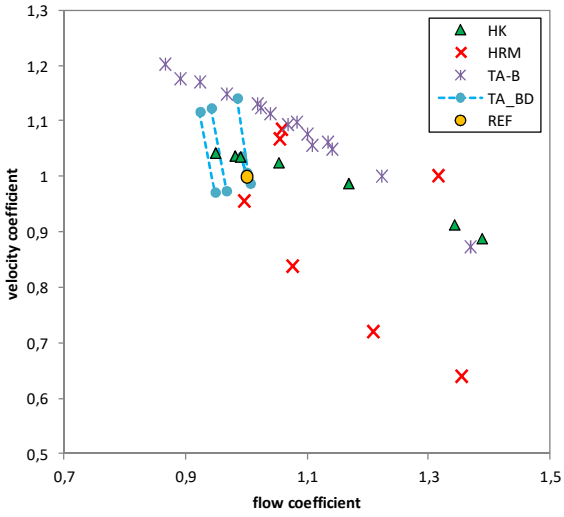

Figure 13 : available flow/velocity solutions by model

Finally the TA-BD model calibration area is marked by blue points in Figure 13. The lines correspond to different N_b values (6.10^{10} max, $3.5.10^{10}$ min); N_d was tested from 1.10^9 to 9.10^{10} values. There was a strong dependence of the flow rate on N_b and velocity on N_d. This resulted in a fairly easy calibration.

Some intermediate conclusion from this analysis:

- HK and TA-B models allow only a narrow band of solution of $\dot{m}$ and V couples. This suggests that the use of 1 or 2 momentum equations does not make any difference regarding the flexibility or robustness of the models
- The number of calibration parameters and their effect on the mass transfer is a key feature of a model for its ability of being calibrated but the type of parameter and sensitivity of the model to it can be very different depending on the formulations

3.3.2.1.3. About physical discrepancies between the models

Regarding the energy equation, the heat transfer between phases was included in all the models. The resulting liquid temperature predictions are shown by Figure 14. For all cases a temperature drop of 30K to 40K was observed depending on the models. In the case of the TA-B and TA-BD models the temperature gradually approaches the saturation temperature when phase change begins (at the throat). Regarding the saturation temperatures profiles, the difference between HRM and TA-BD models comes from the pressure profile difference; since the pressure close to the nozzle outlet was lower for the HRM model, the reference (saturation) temperature is lower than for the TA-BD model. The same observation was done for the HK model close to the nozzle outlet. For that reason, the liquid temperature of HRM and HK models is lower than the one predicted by the TA models. Please note that the sudden saturation temperature increase of HRM model close to the outlet is due to the shock wave mentioned in the comments of the Figure 12; the HK model predicted very similar saturation profile.

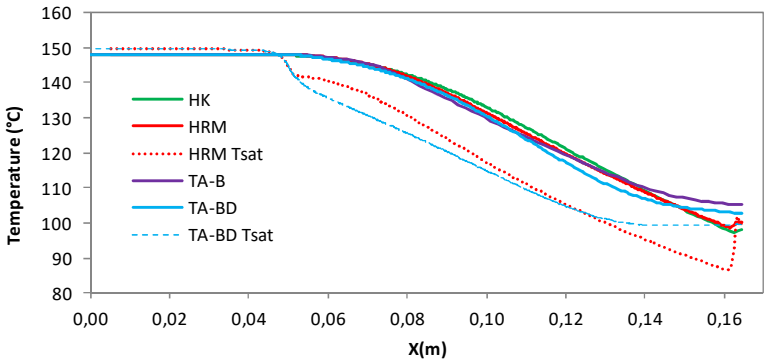

Figure 14 : temperatures at different axial positions; 100kPa outlet pressure

Regarding momentum equation two kinds of models were implemented: the homogeneous (in velocity) and non-homogeneous models. The velocities computed by the different models are shown by Figure 15. It appears that only the homogeneous models give a shock wave even if the velocity magnitudes in the major part of the nozzle are similar to the ones of the non-homogeneous models. Looking at the pressure profiles close to the outlet in Figure 12, it appears that a pressure undershoot of HRM and HK models is related to the velocity overshoot; referring to the pressure measurements it is probable that such a velocity variation in this part of the nozzle does not occur.

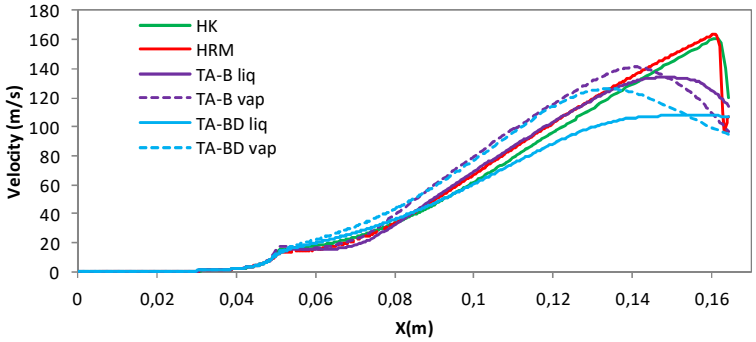

Figure 15 : velocities at different axial positions; 100kPa outlet pressure

Regarding liquid and vapor velocities modeled by the TA-B and TA-BD models one can observe that at the end of the nozzle the vapor is slower than the liquid; that means that the liquid acceleration could not be maintained in a longer nozzle.

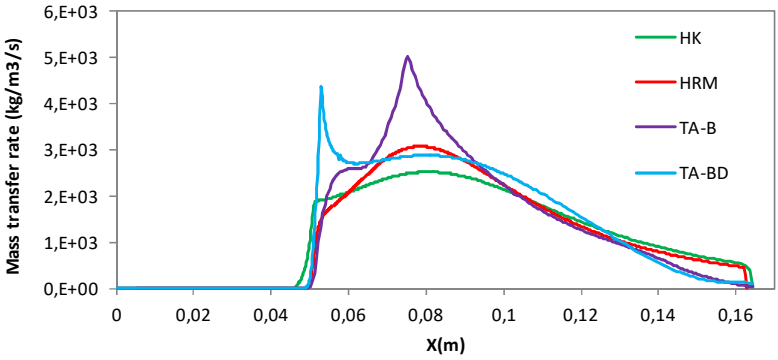

Figure 16 : interfacial mass transfer rate; 100kPa outlet pressure

The interfacial mass transfer rate along the axis of the nozzle is reported in Figure 16. Globally it increases rapidly after the throat, reaches a maximum in the first half of the divergent part and then deceases approaching the outlet. One observes that HK and HRM models compute higher mass transfer rates in the last third of the divergent (0,14m < x < 0,16m) compared to the other models. This difference is related to the interfacial area density formulation of TA-BD and TA-B models that brings it close to zero when void fraction approaches one. The HRM model and HK models produced a sudden decrease of the mass transfer rate in the very last part of the nozzle because of the sudden increase of the pressure after the shock waves.

3.3.2.2. Sub cooling of 12K

In order to observe the sensitivity of the models to a variation in the degree of sub-cooling, the precedent calibrated parameters were maintained for a first simulation series. Then the calibration process was applied as in the precedent section.

The pressure data set was incomplete for this degree of sub-cooling in the referred article for this point. The model discrepancies between the model and measured data are thus shown in terms of mass flow rate and velocity in Table 7. First two lines give the results for the models using the calibration parameters of 1K sub-cooling situation.

Table 7 : summary of errors; Ohta B 12K

		TA-BD	HRM	TA-B	HK
$1K$ SC calibration	er_V	6,8%	22%	24%	17%
	$er_{\dot{m}}$	13%	14%	7,7%	20%
$12K$SC calibration	er_V	2,6%	11%	33%	41%
	$er_{\dot{m}}$	<1%	<1%	<1%	<1%

Form a general point of view, increasing the inlet sub-cooling leads to higher mass flow rate and lower outlet velocities. Qualitatively, this behavior was correctly predicted by all models.

The smallest combined error was produced by the TA-BD model. The predicted mass flow rates and velocities were always higher than measured ones for all the models. TA-B model computed correct mass flow rate but inaccurate velocities.

The last two lines of Table 7 give the flow rate and velocity average discrepancies obtained after calibration. Values of the calibration parameters are given in the Table 8.

Table 8 : calibrated parameters; Ohta B 12K

λ (HK)	Θ_0/a/b (HRM)	N_b/k_h (TA-B)	N_b/N_d (TA-BD)
0,15	$6\,.\,10^{-4}/-0.26/-0.05$	$2\,.\,10^{9}/\,8$	$1{,}1\,.\,10^{12}/9\,.\,10^{8}$

After the calibration step, the mass flow rate obtained by all the models was of 156g/s with less than 1% error. The value of the parameter responsible of the mass flow rate for HK and TA models (λ and N_b) is higher than the value at 1K SC.

Please note the increase in velocity error for TA-B and HK after the mass flow rate calibration step. The reason is that the accommodation coefficients were increased in order to increase the cavitation inception pressure and thus reduce the mass flow rate; consequently the vapor production was increased and so were the velocities. Please refer to Figure 13 to observe the relation between flow rate and velocity for these 2 models. This illustrates the problem of using a unique calibration parameter or several calibration parameters acting in the same way on all the evaporative situations.

The velocities obtained after calibrations are shown in Figure 17; corresponding efficiencies in Figure 18.

The observation about the flexibility of the models can be applied here as well: only TA-BD and HRM were able to give the right outlet velocity at 100kPa outlet pressure during calibration. The most robust model is the TA-BD model.

The efficiency trend (Figure 18) is well captured by all models. TA-BD and HRM models are the closest to the reality. The efficiency plateau closest to the reality is obtained with TA-BD model.

The simulated pressures are shown in Figure 19. One sees similar profile characteristics to the 1K sub-cooling case i.e. a pressure plateau for certain models after the throat and a shock wave in last quarter of the divergent for the two HRM and for HK models.

Regarding the cavitation inception pressure, Ohta observed 2.8bar and 2.1bar pressures for 1K and 12K degrees of sub-cooling respectively. This is close to 0.6 times saturation pressure at inlet temperature. Ohta guessed the inception to occur just after the throat. The computed pressure at this point by the TA-BD model gives a factor relative to saturation pressure close to 0.8; so inception pressure was overestimated.

The assumed N_b values seem to increase when increasing liquid inlet sub-cooling. This is consistent with the result of [14].

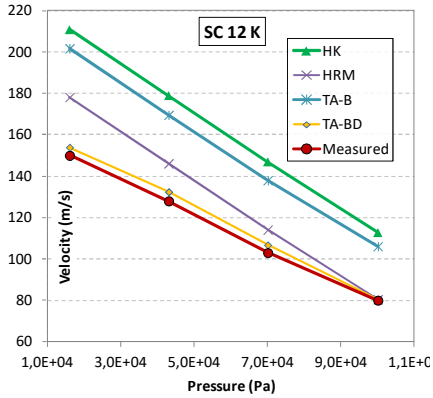

Figure 17 : outlet velocity function of outlet pressure; SC12K;nozzle B; mass flow calibrated models

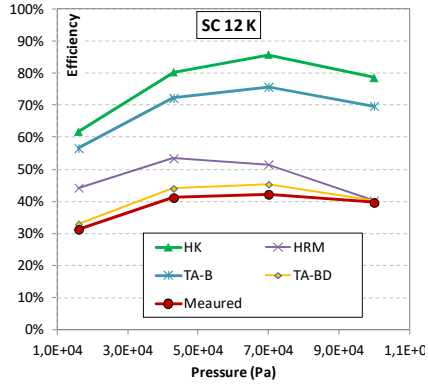

Figure 18 : nozzle efficiency function of outlet pressure; SC12K;nozzle B; mass flow calibrated models

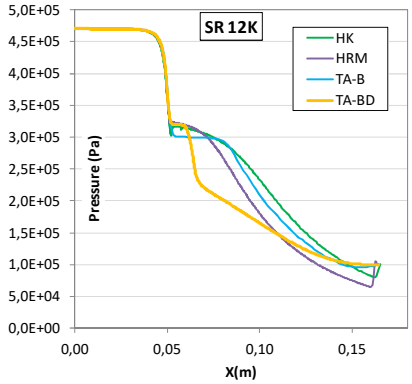

Figure 19 : static pressure profiles; SC12K 1bar outlet pressure; nozzle B; mass flow calibrated models

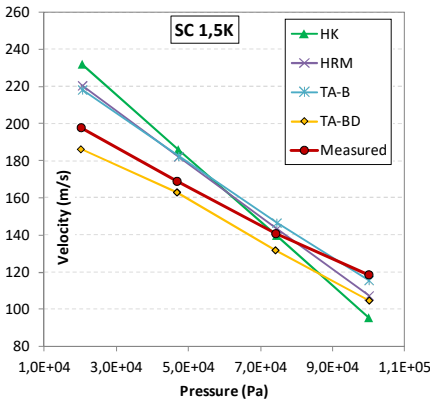

Figure 20 : outlet velocity function of outlet pressure; SC1.5K;nozzle F

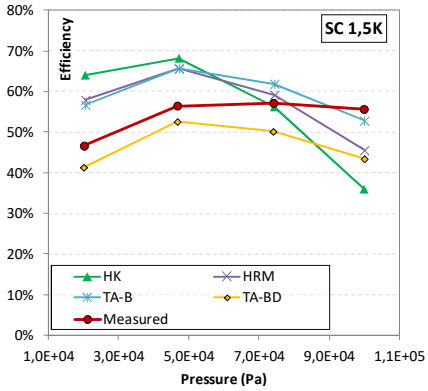

Figure 21 : nozzle efficiency function of outlet pressure; SC12K;nozzle F

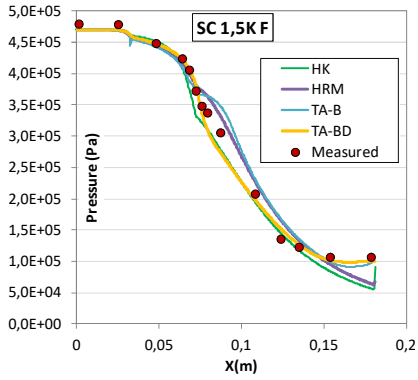

Figure 22 : static pressure profiles; SC1.5K 1bar outlet pressure; nozzle F

3.3.3. Ohta F Nozzle

3.3.3.1. Results summary

The inlet conditions for this nozzle were identical to the first case (1K SC degree). The computations were done supposing that only inlet and outlet conditions affect the phase change regime. The parameters of the models for 1K SC were therefore maintained (the ones of Table 5).

The mean errors for mass flow rate, velocity, and pressure are reported in Table 9. For velocity we give the mean of the four outlet pressures cases. The pressure error is the one of the 100kPa case. The mass flow rate was identical for all the outlet pressures.

Table 9 : summary of errors; Ohta F 1.5K

	TA-BD	HRM	TA-B	HK
$er_{\dot{m}}$	6,3 %	10%	15%	-8,8%
er_V	6,9%	7,6%	6,2%	12%
er_P	5,7%	9,6%	7,8%	10%

The mass flow rates obtained for this nozzle range from 108 g/s to 136 g/s depending on the model; those values are relatively close to the measured rate of 118g/s.

The obtained outlet velocities and corresponding isentropic efficiencies are reported in Figure 20 and Figure 21. The outlet velocity values and global trend are quite good captured by all models but the efficiency maximum was not correctly modeled. The measured values show an efficiency plateau between 45kPa and 100kPa outlet pressures that was not predicted by any model. The efficiency sensitivity to pressure was especially high for HK model. Also, the TA-BD model shows a moderate efficiency variation as was observed by Ohta experiments.

The pressure profiles obtained by the different models for 100kPa outlet pressure are show in Figure 22. A shock wave appears in the last part of the divergent section for HK and HRM models; this resembles to the simulated pressure profiles of the B nozzle. The pressure plateau of the TA-B model is shorter than in the precedent case.

The most close to measurements are the TA-BD and HRM models for this case. The TA-B model gives quite good values for velocity but over estimates the mass flow rate; if one tries to calibrate it by increasing N_b to get the right flow rate, the velocities would increase a lot.

The effect of the geometry on the phase change regime is clearly not negligible; even if some models take it into account relatively well without any supplementary calibration, the efficiency in Figure 21 for the TA-BD model is not satisfactory. The sensitivity of the efficiency to the outlet pressure is quite low compared to the B nozzle and this is not well captured by the tested and proposed models.

Compared to the B nozzle, the higher discrepancies for the F nozzle in terms of efficiency could be explained by a poor formulation of the interfacial area density that would be highlighted in the case of the F nozzle.

3.3.3.2. A flow analysis

The difference between B and F nozzles is the geometry of the convergent part. The length of the small section part is higher in the case of F nozzle and the angle before the throat is lower. This should affect what happens in the divergent part.

In order to analyze the effect of the throat and convergent geometry on the phase change regime and the flow, the contours of the void fraction and degree of superheat are shown in Figure 23 for the B nozzle and in Figure 24 for the F nozzle. The black lines on the images are “isolines” for 0K superheat (Sch) and 2% void fraction (VOF).

In the case of the B nozzle one sees that there is a high Sch close to the throat’s outer radius; this is a favorable situation for phase change close to the wall. In the case of the F nozzle this local Sch increase does not appear and thus the phase change will be more homogeneous.

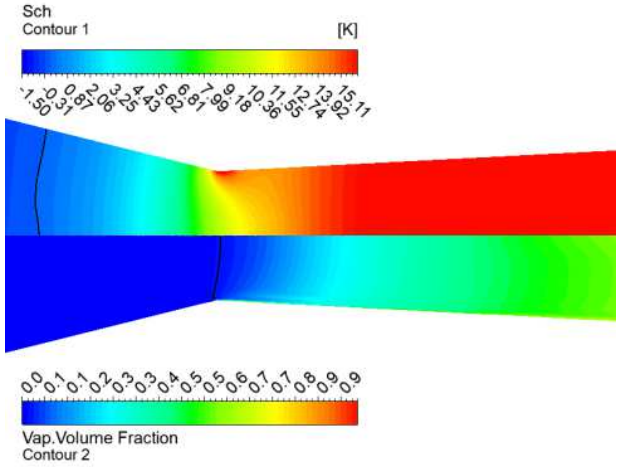

Figure 23 : Ohta B nozzle; 1.5K 100kPa; superheat and void fraction

Furthermore the phase change begins long before the throat for the F nozzle, thus the void fraction at the throat is higher than for the nozzle B; this could explain the lower flow rate of the F nozzle despite its larger throat. It would be useful to confirm this early vapor generation by experimental observations.

One may point out that the formulation of the interfacial area density of the TA-BD model is only function of the void fraction. So despite its globally good results, the formulation is probably not complex enough to model the multitude of topologies constitutive of depressurized phase change flows.

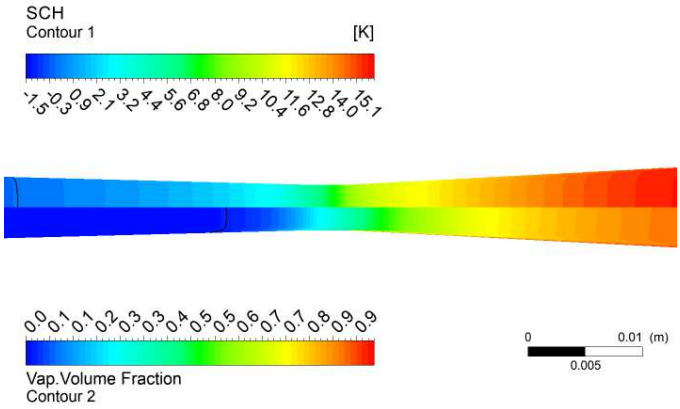

Figure 24 : Ohta F nozzle; 1.5K 100kPa; superheat and void fraction

4. Conclusion and future work

This paper deals with CFD modeling of two phase turbine flash nozzles.

The paper explored the ability of 4 models to predict nozzles' mass flow rate and efficiency. Experimental data specifically containing nozzle outlet velocity measurements were used as reference.

The four models were implemented in the commercial software Ansys CFX i.e. the HK model based on a pressure difference, the HRM model based on a vapor quality difference, the TA-B and TA-BD models based both on a temperature difference but different interfacial area density formulations.

The ability of the 4 models to be calibrated was tested on two nozzle geometries. Three models were based on precedent research works. The last one is a model newly explored in this paper for flash nozzles; this is a variation of the Wu model [15].

From the comparisons with experimental data, it can be observed, concerning the calibration and prediction capacity of the models, that:

- Less than 1% error could be obtained on mass flow rate by all the tested models. The mass flow rate seems to be driven by the vapor generation rate in the region of the 5K to 10K first degrees of superheat.
- The calibration of the mass flow rate is incompatible with the one of the outlet velocity (or efficiency) excepted for the HRM and TA-BD models.
- The mass flow rate is strongly affected by the degree of sub-cooling at the inlet. This effect is captured by all the models but is overestimated. Thus, to improve the precision when the sub-cooling degree changes, models need to be recalibrated. For the models using a single or redundant calibration parameters (HK and TA-B), this produces an increase of the errors on velocity.
- Regarding the HRM model calibration, for a given sub-cooling, the calibration of two parameters seems to be sufficient. The calibration process of the HRM model is quite difficult since the parameters are strongly coupled and the associated effects are non linear.
- Regarding the tested HK-type model, it gave relatively good results but always higher discrepancies in average than other models. This model is limited by the use of a unique adaptation parameter. It should be noticed that the explored transition interfacial area density formulation could be used in HK based models.
- The TA-BD model is the most robust model. Regarding its calibration parameters, the number of bubbles density affects the mass flow rate and the number of droplets density affects the outlet velocity.
- Two nozzle geometries were tested. It was observed that the model that best adapts to geometry change is the TA-BD model. However, the sensibility to the outlet pressure was not well captured by any model for the F nozzle.

The last remark underlines a limitation of the TA-BD model: the interfacial area density formulation does not depend on nozzle geometry; however the interface topology is certainly modified by the nozzle shape. So the interfacial area density formulation should be improved. The shape optimization CFD techniques could be enhanced by this eventual improvement.

Another limit of the TA-BD model is the use of predefined N_b and N_d values. Additional work should be done to integrate a nucleation model to predict N_b. Regarding N_d values, the order of magnitude was similar to the one of N_b values, higher or lower. It is not yet clear how it could be predicted. It may be useful to introduce a droplet breakup model as a function of liquid/gas velocity slip. Also the effect of the boundary conditions uncertainty should be explored by uncertainty propagation simulation analysis in order to obtain the confidence interval of the prescribed calibration parameters.

Acknowledgments

This work was realized thanks to the financing of ADEME (Agence de l'Environement et de la Maîtrise de l'Energie) and Storewatt SAS. The author is also thankful to Florian Dittmann for his careful rereading.

5. References

[1] M. A. Iqbal, S. R. Mahdi, A. A. Date and AliakbarAkbarzadeh, "Experimental study on the prospect of low-temperature heat to power generation using Trilateral Flash Cycle (TFC)," *Applied Thermal Engineering,* vol. 172, 2020.

[2] D. G. Elliott, Theory and Tests of Two-Phase Turbines, Pasadena: Jet Propulsion Laboratory, 1982.

[3] I. K. Smith, "Development of the trilateral flash cycle system. Part 1 : fundamental considerations," *Proc Instn Mech Engrs,* vol. 207, 1993.

[4] M. T. White, "Cycle and turbine optimisation for an ORC operating with two-phase expansion," *Applied Thermal Engineering,* vol. 192, 2021.

[5] S. Rane and L. He, "Numerical analysis of a novel two-phase turbine using thermal non-equilibrium, homogeneous nucleation phase change," *Thermal Science and Engineering Progress,* vol. 22, 2020.

[6] N. Abuaf, "A study of Nonequilibrium Flashing of Water in a Converging-Diverging Nozzle: Volume1. Experimental. U.S. Nuclear Regulatory Comission," 1981.

[7] F. Bussac, "Developpement d'une turbine diphasique pour la production d'électricité à partir de la détente de saumures géomethermales," Commission des Communautés européennes, 1985.

[8] M. Haida, J. Smolka, A. Hafner, M. Palacz, K. Banasiak and A. J. Nowak, "Modified homogeneous relaxation model for the R744 trans-critical flow in a two-phase ejector," *International Journal of Refrigeration,* pp. 314-333, 2017.

[9] F. Giacomelli, F. Mazzelli and A. Milazzo, "A novel CFD approach for the computation of R744 flashing nozzles in compressible and metastable conditions," *Energy,* vol. 162, pp. 1092-1105, 2018.

[10] B. M. Devassy, D. Benković, Z. Petranovic, W. Edelbauer and M. Vujanovic, "Numerical Simulation of Internal Flashing in a GDI Injector Nozzle," in *Conference on Liquid Atomization and Spray Systems*, Paris, 2019.

[11] I. Karathanassis, "Comparative evaluation of phase change mechanisms for prediction of flashing flows," *International Journal of Multiphase Flows,* vol. 97, pp. 257-270, 2017.

[12] L. Yixiang and L. Dirk, "Computational modelling of flash boiling flows, a literature survey," *International Journal of Heat and Mass Transfer,* pp. 246-265, 2017.

[13] P. Downar-Zapolski and Z. Bilicki, "The non-equilibrium relaxation model for one-dimensional flashing liquid flow," *International Journal of Multiphase Flow,* vol. 22, pp. 473-483, 1996.

[14] L. Yixiang and L. Dirk, "3D CFD simulation of flashing flows in a converging-diverging nozzle," *Nuclear Engineering Design,* pp. 149-163, 2015.

[15] A. N. Wu B.J.C., "A study of Nonequilibrium Flashing of Water in a Converging-Diverging Nozzle: Volume2. Modelling. U.S. Nuclear Regulatory Comission," 1981.

[16] J. Ohta, T. Fuji, K. Akagawa and N. Takenaka, "Performance and flow characteristics of nozzles for initially subcooled hot water (influence of turbulence and decompression rate)," *International Journal of Multiphasse Flow,* vol. 19, no. 1, pp. 125-136, 1993.

[17] Ansys, Fluent V20 Users Guide, 2020.

[18] M. Yazdani, T. D. Radcliff, A. A. Alahyari and M. Farzad, "Numerical Modeling and Validation so Supersonic Two-Phase Flow of CO2 in Converging-Diverging Nozzles," *Journal of Fluid Engineering,* vol. 136, 2014.

[19] Q. D. Le, FLASHING FLOW MODEL FOR INDUSTRIAL ENERGY APPLICATIONS, POLITECNICO DI MILANO, 2017.

[20] G. Palau-Salvador, P. Gonzalez-Altozano and J. Arviza-Valverde, "Numerical modeling of cavitating flows for simple geometries," *Spanish Journal of Agricultural Research,* 2007.

[21] M. Palacz, M. Haida, J. Smolka, A. J. Nowak, K. Banasiak and A. Hafner, " HRM accuracy comparison for the simulation of CO2 expansion in two-phase ejectors for supermarket refrigeration systems," *Applied Thermal Engineering,* no. 115, pp. 160-169, 2017.

[22] S. Maksic and D. Mewes, "CFD-CALCULATION OF THE FLASHING FLOW IN PIPES AND NOZZLES," *Proceedings of ASME FEDSM'02,* 2002.

[23] L. Geng, H. Liu and X. Wei, "CFD analysis of the flashing flow characteristics of subcritical refrigerant R134a through converging-diverging nozzles," *International Journal of Thermal Sciences,* pp. 438-445, 2019.

[24] H. Guo, L. Nocivelli, R. Torelli and S. Som, "Towards understanding the development and characteristics of under-expanded flash boiling jets," *International Journal of Multiphase Flow,* 2020.

[25] A. M. SINGHAL A.K., "Mathematical bases and validation of the full cavitation model," *J Fluids Eng,* vol. 124, pp. 617-624, 2002.

[26] M. S. Lee, H. Lee, Y. Hwang, R. Radermacher and H.-M. Jeong, "Optimization of two-phase R600a ejector geometries using a non-equilibrium CFD model," *Applied Thermal Engineering,* vol. 109, no. 26, pp. 272-282, 2016.

[27] M. D. Lorenzo, P. Lafon, M. D. Matteo, M. Pelanti, J.-M. Seynhaeve and Y. Bartosiewicz, "Homogeneous two-phase flow models and accurate steam-water table look-up method for fast transient simulations," *International Journal of Multiphase Flow,* pp. 199-219, 2017.

[28] W. Angielczyk, Y. B. D. Brtosiewicz and J.-M. Seynhaeve, "1-D Modeling of Supersonic Carbon Dioxide Two-Phase Flow Through Ejector Motive Nozzle," in *Internation Refrigeration and Air Conditioning Conference*, Purdue, 2010.

[29] A. A. Avdeev, "Laws of Vapor Bubble Growth in the Superheated Liquid Volume (Thermal Growth Scheme)," *High Temperature,* vol. 52, no. 4, pp. 588-602, 2014.

[30] E. Krepper, L. Dirk, T. Frank, H.-M. Prasser and J. Zwart Phil, "The inhomogeneous MUSIG model for the simulation of polydispersed flows," *Nuclear Engineering and Design,* no. 238, pp. 1690-1702, 2008.

[31] S. Hänsch, D. Lucas, E. Krepper and T. Höhne, "A multi-field two-fluid concept for transitions between different scales of interfacial structures," *International Journal of Multiphase Flow,* vol. 47, pp. 171-182, 2012.

[32] Ansys, CFX V20 User's Guide, 2020.

[33] J. Sende, Y. Hojyo and H. Fujimoto, "Modeling on atomization and vaporization process in flash boiling spray," *JSAE Review,* vol. 15, pp. 291-296, 1994.

597

598